Oxidized Porous Silicon Nanostructures Enabling Electrokinetic Transport for Enhanced DNA Detection

Rita Vilensky, Moran Bercovici, and Ester Segal**

Nanostructured porous silicon (PSi) is a promising material for the label-free detection of biomolecules, but it currently suffers from limited applicability due to poor sensitivity, typically in micromolar range. This work presents the design, operation concept, and characterization of a novel microfluidic device and assay that integrates an oxidized PSi optical biosensor with electrokinetic focusing for a highly sensitive label-free detection of nucleic acids. Under proper oxidation conditions, the delicate nanostructure of PSi can be preserved, while providing sufficient dielectric insulation for application of high voltages. This enables the use of signal enhancement techniques, which are based on electric fields. Here, the DNA target molecules are focused using an electric field within a finite and confined zone, and this highly concentrated analyte is delivered to an on-chip PSi Fabry–Pérot optical transducer, pre-functionalized with capture probes. Using reflective interferometric Fourier transform spectroscopy real-time monitoring, a 1000-fold improvement in limit of detection is demonstrated compared to a standard assay, using the same biosensor. Thus, a measured limit of detection of 1×10^{-9} M is achieved without compromising specificity. The concepts presented herein can be readily applied to other ionic targets, paving way for the development of other highly sensitive chemical and biochemical assays.

1. Introduction

Since the pioneering work of Sailor and co-workers on porous silicon (PSi) optical biosensors,[1–3] extensive research has been directed toward the development of label-free detection schemes which are based on this technology.[4–6] PSi nanoarchitectures can be easily fabricated by electrochemical anodization techniques. The resulting nanostructured materials exhibit large surface area, which is readily accessible to a wide repertoire of chemical and biological modifications, combined with unique photonic properties.[3,5–12] A wide diversity of optical structures ranging from simple Fabry–Pérot thin films to more complicated multilayered structures, such as photonic crystals, have been designed and utilized for biosensing applications.[1,11,13–17] Despite the significant advantages of optical PSi biosensors, and while theoretical calculations predict detection in the nanomolar range,[18] in practice PSi biosensors exhibit inferior performance with a typical limit of detection (LoD) in the micromolar range.[4,6,11] This discrepancy is mainly attributed to nonideal structures (defects and interface roughness), and limited mass transport of molecules within the porous media.[19,20] Extensive research efforts to improve the performance of PSi biosensors, specifically their sensitivity, have focused on designing sophisticated optical structures, e.g., multilayered 1D and 2D photonic crystals,[21,22] nonperiodic multilayered structures as Thue–Morse and Cantor,[14] and other architectures.[17,23,24]

Detection of a wide range of biomolecular targets, including oligonucleotides,[3,13,16,24–27] proteins,[15,28–30] enzymes,[8,31] and cells,[32] has been reported using PSi biosensors. While detection of DNA targets is of critical importance in numerous applications, including clinical diagnosis, environmental monitoring, and antibioterrorism,[33,34] its sensitive and reproducible monitoring using PSi biosensors is challenging mostly due to the enhanced corrosion of the PSi scaffold by DNA.[25,27,35] To date, the lowest measured LoD for DNA detection using PSi Fabry–Pérot is $\approx 6 \times 10^{-6}$ M,[13] and efforts have been directed toward enhancing sensitivity by applying different passivation chemistries and designing more complex optical devices.[16,18,26,27,36–38] Indeed, Weiss and co-workers were able to accomplish DNA detection in sub micromolar range by employing sophisticated optical nanostructures and advanced optical measurement configurations.[16,27,39]

The integration of PSi-based biosensors with microfluidic systems has gained considerable interest in recent years.[38,40,41] The incorporation of PSi biosensors into lab-on-a-chip devices has shown great promise for sensitive and real-time detection of DNA, offering significant advantages in terms of high throughput, small sample volumes, and rapid operation time.[37,38,40] In addition to these conventional advantages attributed to miniaturization, microfluidic lab-on-a-chip platforms

R. Vilensky, Prof. M. Bercovici, Prof. E. Segal
Russell Berrie Nanotechnology Institute
Technion – Israel Institute of Technology
Haifa 3200003, Israel
E-mail: mberco@technion.ac.il;
esegal@tx.technion.ac.il
Prof. M. Bercovici
Faculty of Mechanical Engineering
Technion – Israel Institute of Technology
Haifa 3200003, Israel
Prof. E. Segal
Faculty of Biotechnology and Food Engineering
Technion – Israel Institute of Technology
Haifa 3200003, Israel

DOI: 10.1002/adfm.201502859

allow for implementation of a variety of electrokinetic techniques.[42,43] Isotachophoresis (ITP) is a simple and robust electrokinetic technique that can achieve as much as a million-fold preconcentration, efficient separation, and extraction based on ionic mobility.[44–46] The analyte of interest is focused at the interface of two distinct electrolyte solutions resulting in a finite zone of highly concentrated analyte. Typically, ITP is performed on nonconductive planar substrates (e.g., glass and plastics),[44,47–49] while recently successful ITP focusing was also demonstrated in porous media such as paper.[50,51]

In this work, we design a novel proof-of-concept assay that interfaces PSi Fabry–Pérot interferometry with ITP and demonstrates its applicability for highly sensitive optical detection of DNA oligonucleotides. Conventionally, highly conductive Si substrates are incompatible with ITP, as during focusing, high voltages are applied. While PSi oxidation is commonly performed for chemical stabilization and hydrophilization of the substrate,[52–54] the quality of these oxide layers is inadequate for electrical insulation. To overcome these limitations, we designed a fabrication and oxidation process of PSi, resulting in a robust insulating oxide layer while preserving the delicate nanostructure characteristics, which are crucial for optical biosensing.

We use ITP to focus the target DNA molecules within a moving ITP plug and precisely deliver it to the PSi biosensor. This highly concentrated DNA plug is held stationary onto the oxidized PSi ($PSiO_2$) scaffold to facilitate efficient diffusion and hybridization. These binding events, occurring within the $PSiO_2$ nanostructure, are monitored in real-time using reflective interferometric Fourier transform spectroscopy (RIFTS).[15] We demonstrate detection of 15 base pairs (bp) DNA hybridization at concentrations as low as 1×10^{-9} M, showing three orders of magnitude enhancement in the sensitivity of PSi-based Fabry–Pérot biosensors. To the best of our knowledge, this is the lowest DNA concentration measured by PSi biosensors. The concepts presented in this work are highly generic and could be applied for the detection of many other relevant biological targets.

2. Results and Discussion

2.1. Principles of the Assay

The underlying principle of the assay is based on two main elements: a $PSiO_2$ Fabry–Pérot interferometer and electrophoretic sample focusing by ITP. **Figure 1** presents a schematic illustration of the microfluidic device and assay.

As illustrated in Figure 1a, our microfluidic device is composed of an oxidized Si substrate which contains a (oxidized) porous region, serving as the sensor. A polydimethylsiloxane (PDMS) layer containing a microchannel structure covers the Si, such that the channel passes precisely on top of the sensor. The surface of the $PSiO_2$ is functionalized with DNA capture probes, containing a sequence that matches the desired target.

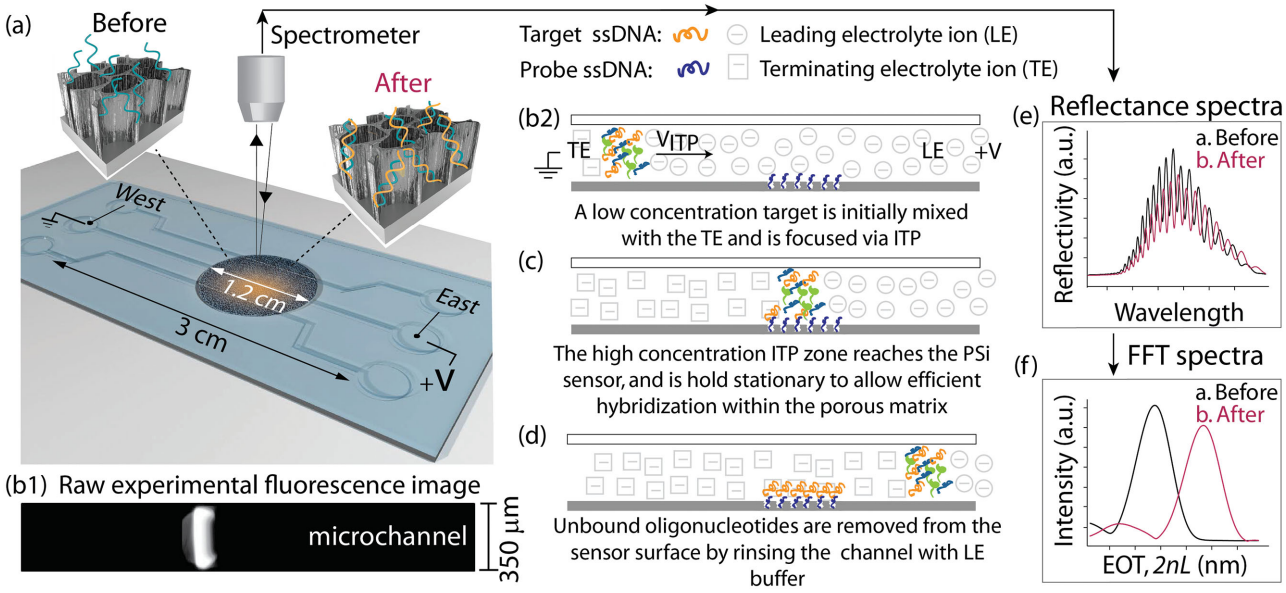

Figure 1. Schematic illustration of the integrated $PSiO_2$ microfluidic system. a) The $PSiO_2$ microfluidic device is composed of two layers; the bottom layer is a heavily doped Si substrate containing a 1.2 cm diameter porous region, oxidized to minimize its electric conductance. The top layer is fabricated out of PDMS and contains a 3 cm long, 350 µm wide, 25 µm deep channel. The two layers are bonded by plasma activation, such that the channel passes over the $PSiO_2$ region. The $PSiO_2$ thin film is prefunctionalized with specific single-stranded DNA (ssDNA) probes to capture the target ssDNA. b1) A raw fluorescence image of labeled oligonucleotides isotachophoretically focused in the channel. b2) Target molecules (ssDNA) are focused under ITP and electromigrate toward the sensor surface. c) The concentrated sample arrives at the $PSiO_2$ site, and is held stationary by applying a pressure driven counter-flow. The complementary sequence binds to the immobilized probe DNA. d) Unbound oligonucleotides are removed from the sensor surface by rinsing the channel with leading electrolyte (LE) buffer. e) The reflectivity spectrum of the $PSiO_2$ results in a red shift of the spectrum due to binding of the complementary ssDNA. f) The effective optical thickness (EOT), is measured via FFT of the spectrum and shows a pronounced increase upon target capture.

To deliver a highly concentrated sample to the sensor site, we leverage the negative charge of nucleic acids to focus target sequences under ITP. The technique uses a discontinuous buffer system consisting of leading electrolyte (LE) and terminating electrolyte (TE). The LE and TE ions are chosen to have respectively higher and lower electrophoretic mobility than the analyte of interest. When voltage is applied along the channel, a sharp electric field gradient is formed at the interface of the LE and TE. Any species having an intermediate electrophoretic mobility focuses at this interface. When sample is mixed with the TE (semi-infinite sample injection), nucleic acid continuously accumulates at the interface, resulting in a rapid increase in its local concentration. In our system, the microfluidic channel and the East reservoir are initially filled with LE buffer, and the West reservoir is filled with TE buffer (see Figure 1a). Target DNA is injected into the West reservoir and is mixed with the TE. Applying an electric field across the channel results in formation of a highly concentrated DNA zone at the narrow LE–TE interface, which electromigrates along the channel. As the concentrated peak reaches the $PSiO_2$ surface, we apply pressure driven flow to counter the electromigration. The highly concentrated target is thus held stationary over the $PSiO_2$, enhancing the diffusion flux into the porous scaffold. The diffusion and subsequent hybridization of the DNA within the nanostructure result in a measurable change in the $PSiO_2$ reflectivity spectrum, which we monitor via RIFTS.[15] Briefly, under perpendicular white light illumination the $PSiO_2$ exhibits a reflectivity spectrum, which consists of the Fabry–Pérot fringe interference pattern, resulting from multiple reflections of light at the top and at the bottom of the porous layer.[3] Applying a frequency analysis (fast Fourier transform, FFT) to the data typically results in a single peak, whose dimension corresponds to the value of the effective optical thickness (EOT), $2nL$, where n is the effective refractive index and L is the physical thickness of the porous layer.[15] Hybridization of the free DNA with its complementary capture probes, which are immobilized within the $PSiO_2$, leads to a change in the average refractive index of the porous layer that correlates with a measurable EOT changes.

2.2. Fabrication and Functionalization of Oxidized PSi

Formation of an isolating oxide layer, capable of withstanding high electric fields, is essential for performing an effective ITP on highly doped Si. Therefore, we carefully optimized the thermal oxidation conditions in order to obtain a robust nonconductive oxide layer, yet maintain the integrity of the delicate porous nanostructure. **Figure 2**a,b depicts cross-sectional and top-view high-resolution scanning electron microscopy (HRSEM) images (secondary electrons) of the $PSiO_2$ film, revealing a highly porous nanostructure, with characteristic interconnecting cylindrical pores ranging in diameter from 60 to 80 nm. Thus, confirming that the severe oxidation process (at 1000 °C for 46 h under constant oxygen flow) did not induce significant morphological changes in the porous nanostructure. Nevertheless, the oxidation leads to a decrease of 7% in the porosity and 15% in the thickness of $PSiO_2$ layer, in comparison to the neat PSi. This decrease is attributed to the volume expansion of the material during oxidation.[55] Conventional thermal oxidization of PSi is carried out at 500–900 °C for durations of several minutes to an hour,[11,52,56–59] primarily to improve the nanostructure stability in aqueous media. Oxidation at temperatures higher than 1000 °C leads to structural deterioration of the porous layer, accompanied by drastic decrease in the surface area and transition of the elongated columns into closed sphere-like pores;[60–62] thus unsuitable for biosensing applications. Indeed, we found that oxidation at temperatures above 1010 °C caused severe structural changes (see Figure S1, Supporting Information), resulting in a drastic decrease in the thickness and the porosity of the porous layer, and eventually collapse of the nanostructure.[60] By lowering the oxidation temperature to 1000 °C and extending its duration to 46 h, we achieve complete oxidation of the porous layer and formation of a 850 nm thick planar SiO_2 layer beneath the oxidized porous nanostructure, while preserving the delicate nanostructure of the porous layer. These characteristics can be seen in Figure 2c, presenting a cross-sectional backscattered electron micrograph of the $PSiO_2$ film, which provides elemental composition contrast. The appearance of the planar oxide layer can be clearly observed in the FFT spectrum of the film (see inset Figure 2c).[15]

Functionalization of the $PSiO_2$ sensor requires multiple steps, some of which we carried out on the neat $PSiO_2$ substrate,

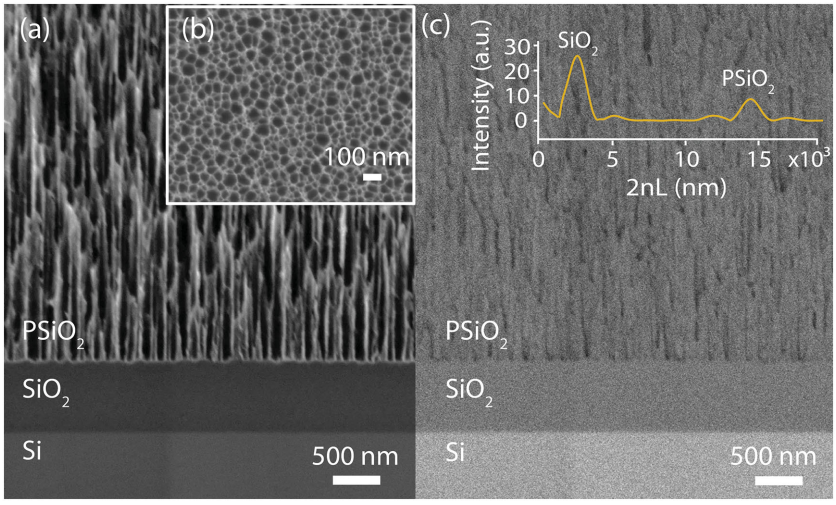

Figure 2. HRSEM micrographs of the $PSiO_2$ film. a,b) Cross-sectional and top-view images of the oxidized porous film (secondary electrons imaging), revealing a highly porous nanostructure with characteristic interconnecting cylindrical pores ranging from 60 to 80 nm in diameter, confirming that the porous nanostructure characteristics are maintained in spite of the severe oxidation process. c) Cross-sectional image of porous film acquired using a backscattered electron detector, providing elemental composition contrast. Distinct contrast differences are observed for oxidized versus nonoxidized fractions of the film. The lower brightest part of the image corresponds to the planar Si, while the darker regions to the planar Si oxide and $PSiO_2$. The inset shows the FFT spectrum of the oxidized film, depicting two distinct peaks at 2550 and 14360 nm, corresponding to the planar SiO_2 and $PSiO_2$ thin films, respectively.

and some we performed after assembly with the microfluidic channel. Specifically, we performed silanization on bare $PSiO_2$, and subsequent surface modification steps, including cross-linker and probe DNA conjugation, within the microfluidic channel. We used RIFTS for real-time monitoring of the immobilization of the thiol-modified ssDNA probe to the presilanized $PSiO_2$. Figure S2 (Supporting Information), presents the relative ΔEOT changes during the process, confirming successful conjugation of the DNA probe.

2.3. Demonstration and Characterization of ITP Focusing on Oxidized PSi

In general, highly doped Si platforms are considered to be incompatible with electrokinetic assays due to their high surface conductance. Herein, we demonstrate that by appropriate oxidation we are able to render the conductive PSi substrate to withstand moderate voltages, applied during electrokinetic assays. **Figure 3**a presents the concentrated target ssDNA zone (of initial concentration values of 1×10^{-9}, 10×10^{-9}, and 100×10^{-9} M) formed under electrophoretic focusing on the functionalized $PSiO_2$. The focusing effect is clearly observed

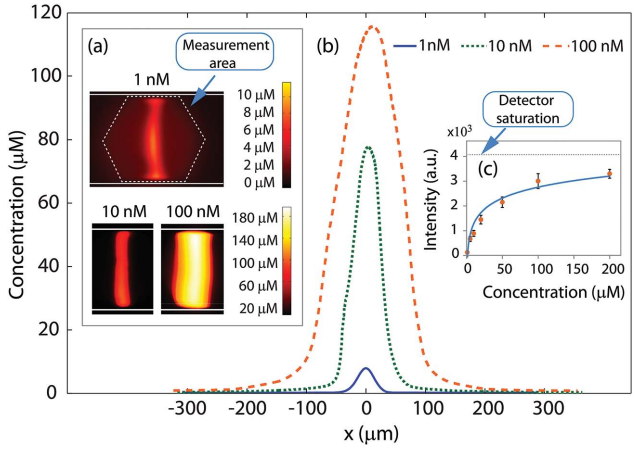

Figure 3. a) Concentration distributions of fluorescently labeled ssDNA molecules focused by ITP on the ssDNA-functionalized $PSiO_2$ film at initial concentration of 1×10^{-9}, 10×10^{-9}, and 100×10^{-9} M. We confine the imaging area to the inner region of the microchannel by using the microscope's iris, as depicted by the dashed line polygon. This area of the $PSiO_2$ region is subsequently monitored during RIFTS. b) Width-averaged concentration profiles of the analyte for initial concentrations of 1×10^{-9}, 10×10^{-9}, and 100×10^{-9} M. The curves represent an average of three images obtained from different devices and experiments. The maximum peak concentration obtained for each of the three runs at each concentration is: 1×10^{-9} M: 5.7, 6.2, 7.3; 10×10^{-9} M: 67, 80, 76; 100×10^{-9} M: 105, 128, 110. The ITP peak concentration profile obtained for 100×10^{-9} M does not represent the actual analyte concentration, as the fluorescent signal obtained under ITP focusing is self-quenched due to the resulting high concentration. c) Calibration curve relating known concentrations of fluorescently labeled ssDNA (1×10^{-6}, 5×10^{-6}, 10×10^{-6}, 20×10^{-6}, 50×10^{-6}, 100×10^{-6}, and 200×10^{-6} M) to the measured intensity. The calibration curve reaches saturation at about 100×10^{-6} M due to self-quenching of the dye (importantly, the camera was far from saturation under the imaging conditions). We fitted the data to an exponential trend line, which we used as the calibration curves to measure the concentration of the DNA within the ITP peak.

and the concentrated peak is well established across all concentrations examined. In order to determine the actual ssDNA concentration within the focused ITP peak, we converted the fluorescence images from intensity to concentration values by using a separately constructed calibration curve (Figure 3c). For initial concentrations of 1×10^{-9} and 10×10^{-9} M, the achieved maximal local concentrations are 9×10^{-6} and 100×10^{-6} M (see Figure 3a), respectively, providing a 10 000 enhancement in concentration. For an initial concentration of 100×10^{-9} M, direct quantification of the ITP concentration was not possible due to self-quenching encountered at high concentrations (see calibration curve in Figure 3c). However, based on the focusing factors obtained at lower concentrations, we evaluate the maximum ITP concentration in this case to be 1×10^{-3} M. Figure 3b presents the width-averaged concentration profiles for the three cases, providing quantitative evaluation of the ITP profile.

ITP is typically performed on nonconductive, flat surfaces such as glass.[44,46,49] Recently, Rosenfeld and Bercovici have described an analytical model for ITP in porous media (paper) and introduced a simple figure of merit for evaluating and comparing the efficiency of ITP on different substrates.[50] This figure is defined as $\eta = N_a(t)/c_a^0 \int_0^t I(\tau)d\tau$, where $N_a(t)$ is the number of sample molecules accumulated at the interface, $\int_0^t I(\tau)d\tau$ is the total amount of charge which passed in the system, and c_a^0 is the initial concentration of the analyte in the reservoir. We calculate the total accumulated sample, $N_a(t)$, by integrating the width-averaged concentration with a threshold of 10% of the peak and multiplying it by the corresponding volume, accounting for both the depth of channel (with a porosity of 1) and for the $PSiO_2$ film (with a measured porosity of 0.74). The electric current integral can be readily obtained from the continuous current measurements recorded by the sourcemeter. For ITP on $PSiO_2$, we obtained η value of 0.8×10^{-4} L A^{-1}s^{-1}, which is of the same order of magnitude as that measured in glass by Rosenfeld and Bercovici, $\eta_{glass} = 1.3 \times 10^{-4}$.[50] We attribute the deviation of η_{PSiO_2} from that of glass to loss of target molecules due to some adsorption during the propagation of the ITP front onto the functionalized $PSiO_2$ substrate. This adsorption of the fluorescently labeled ssDNA to the functionalized $PSiO_2$ is clearly observed during the ITP migration. Since in our assay, the porous region occupies ≈30% of the channel's length (see schematic illustration in Figure 1a), the ITP mainly propagates on top of planar SiO_2, and thus the decrease in η is not significant. Hence, by optimizing the configuration of our device to minimize the $PSiO_2$ region can potentially increase the ITP efficiency.

2.4. Optical Biosensing under ITP-Based Hybridization

We here demonstrate the compatibility of ITP-based hybridization with optical detection (via RIFTS), and its contribution toward reduction of limits of detection. In our RIFTS experiments, we expose the ssDNA-functionalized-$PSiO_2$ to the complementary ssDNA solution, monitor the reflectivity spectra of the porous film in real time, and compute the corresponding EOT values. In this proof-of-concept, the ssDNA molecules are fluorescently labeled. It should be emphasized that this labeling is used for visualization of the ITP peak only,

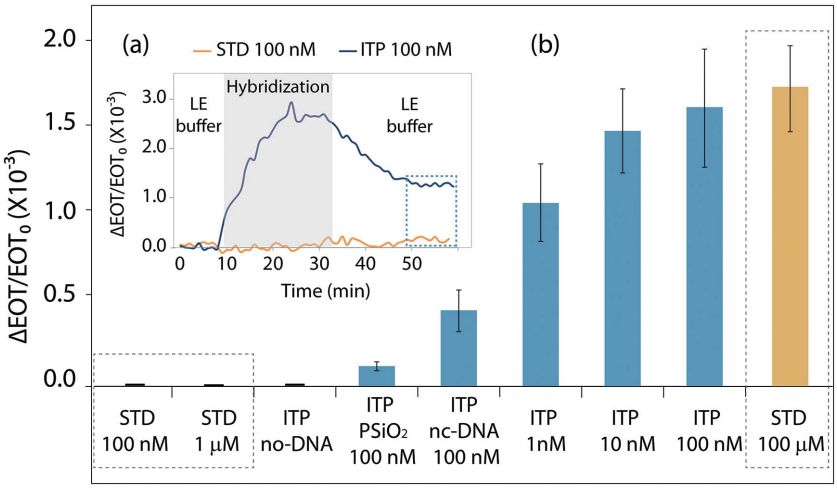

Figure 4. a) Real-time RIFTS monitoring of the relative ΔEOT during standard hybridization versus ITP-based hybridization at an initial concentration of 100×10^{-9} M. After a stable baseline was obtained in the leading electrolyte (LE), the biosensor was exposed to the complementary ssDNA in LE (standard assay) or to the concentrated ITP peak (ITP-based assay). While standard hybridization did not induce a detectable EOT shift, the ITP-based hybridization resulted in a significant increase in EOT signal. During the ITP-based hybridization, a rapid increase in the relative ΔEOT was observed until a stable signal was attained. Upon rinsing of the channel with LE buffer, nonhybridized DNA was removed from the biosensor until a steady state was achieved in which the signal corresponds to hybridized DNA. b) Steady state relative ΔEOT values for standard hybridization (STD 100×10^{-9} M, 1×10^{-6} M, and 100×10^{-6} M) and ITP-based hybridization (ITP 1×10^{-9}, 10×10^{-9}, and 100×10^{-9} M). While no significant signal is obtained for standard hybridization at 1×10^{-6} M, a distinct signal is observed for ITP-based hybridization at 1×10^{-9} M, showing a three order of magnitude improvement in limit of detection. Using 100×10^{-9} M of noncomplementary DNA (ITP nc-DNA) results in a signal lower than that of 1×10^{-9} M complementary DNA, indicating the specificity of the assay. Performing the same experiment on neat (nonfunctionalized) $PSiO_2$ indicates that the level of nonspecific binding to the substrate makes up only a small fraction of nonspecific binding. In the absence of any target molecules (ITP no-DNA), no detectable difference in EOT is obtained at steady state, indicating that the ITP buffer system itself does not affect the signal.

while the DNA detection is based on label-free reflectivity measurements.

Figure 4a presents the change in the relative ΔEOT values as a function of time upon introduction of 100×10^{-9} M complementary DNA, for both standard and ITP-based hybridizations. Under standard incubation with the target, no shift in the EOT was observed. These results are in agreement with previous studies of Fabry–Pérot PSi-based biosensors in which the limit of detection of DNA hybridization was observed to be 6×10^{-6} M.[13] In contrast, in the ITP-based assay, in which the complementary ssDNA was delivered to the functionalized $PSiO_2$ region as a concentrated zone, a significant increase in the EOT was observed until saturation was attained. This increase is attributed to the infiltration of the ssDNA molecules into the pores and their hybridization to the complementary immobilized probe. When rinsing the channel with LE buffer, nonhybridized ssDNA targets leave the pores, resulting in a decrease in the EOT until a stable value was obtained. Accordingly, this steady state EOT shift (mean value of 1.6, corresponding to a net value of 26 nm) is ascribed to the surface-bound targets and constitutes the relevant readout signal of the assay. It should be noted that previous studies on PSi-based DNA biosensors have reported on a blue shift in the reflectance spectra upon DNA introduction (both, probe and target).[3,25,27] This is ascribed to an undesired DNA-induced dissolution of the porous scaffold.[25,27] In our work however, decrease in EOT was not observed during the time span of the assay (see Figure 4a), typically 20 min, in spite of the high concentration of the target DNA molecules introduced during ITP focusing. This may be attributed to the harsh oxidation conditions of the porous scaffold, resulting in a thick (850 nm) and robust insulating oxide layer. This oxide film serves as a passivating layer which delays the corrosion of the porous film.

Figure 4b summarizes the steady-state relative ΔEOT values measured under standard conditions for initial concentrations of 100×10^{-9} M, 1×10^{-6} M, and 100×10^{-6} M, and under ITP at initial target concentrations of 1×10^{-9}, 10×10^{-9}, and 100×10^{-9} M. The data show that under ITP, significant EOT increase was obtained for all three concentrations examined, where the lowest concentration detected in our system is 1×10^{-9} M. At the same time, standard hybridization at 1×10^{-6} M does not yield a significant signal. This represents a three orders of magnitude enhancement in sensitivity in comparison to standard hybridization and to previously reported Fabry–Pérot PSi-based biosensors.[13,16] Furthermore, the ΔEOT obtained in standard hybridization at 100×10^{-6} M is equivalent to that obtained in ITP at 100×10^{-9} M.

Quantitative measurement is obtained between 1×10^{-9} and 10×10^{-9} M, whereas saturation of the hybridization sites is observed above 10×10^{-9} M. In our experiments, we did not test concentrations lower than 1×10^{-9} M. However, we expect the LoD to be lower than 1×10^{-9} M, based on the significant EOT changes observed at this concentration (see Figure 4b). Importantly, to rule out possible EOT changes due to the complex buffers system used in ITP, we have characterized the biosensor's response to a negative control case in which ITP was conducted without target DNA. As shown in Figure S3 (Supporting Information), the relative ΔEOT achieved at steady state was negligible.

To examine the specificity of the assay, we performed the assay using a noncomplementary ssDNA strand (5′-TGATTCAAGCCGACT-FITC-3′). Figure 4b compares the relative ΔEOT obtained at steady state for noncomplementary versus complementary DNA sequences, using an initial concentration of 100×10^{-9} M. The biosensor showed an average relative ΔEOT of 1.6 for the complementary ssDNA in comparison to a value of 0.4 for the noncomplementary sequence. Notably, the latter is significantly lower than the signal obtained even at 1×10^{-9} M of the complementary (Figure 4b). This significant difference (t-test, $p < 0.05$) demonstrates the specificity of the assay. The partial nonspecific hybridization observed may be attributed to the high DNA concentration under ITP focusing (evaluated to be $\approx 1 \times 10^{-3}$ M), which is one order of magnitude lower than the dissociation constant of the reaction.

It is also important to determine to what extent nonspecific adsorption of the ssDNA to the surface contributes to the observed signal. This is particularly important for our oxidized $PSiO_2$, as it is well-established that under certain conditions of ionic strength and pH, DNA molecules tend to adsorb onto silica surfaces.[63] Although, our $PSiO_2$ biosensor is silanized to allow conjugation of the ssDNA probe, surface coverage is likely to be incomplete[27] and thus bare oxide regions may be susceptible to nonspecific adsorption. Figure 4b presents the results obtained for ITP performed on neat $PSiO_2$ (not functionalized). Small relative ΔEOT changes (0.12) were detected for this case, indicating very little adsorption. This result further supports the previous conclusion, which ascribes the biosensor response to the mismatch sequence to nonspecific hybridization, rather than to nonspecific adsorption.

3. Conclusions

This is the first report demonstrating the compatibility of PSi-based optical transducers with electrokinetic assays. To render the highly conductive Si compatible with applications of electric fields in the channel, the Si scaffold must be carefully oxidized to obtain a thick and robust insulating oxide layer, while preserving the morphological characteristics of the delicate nanostructure. We demonstrated that ITP-based hybridization results in significant and well-defined changes in the $PSiO_2$ optical reflectivity spectrum at concentrations as low as 1×10^{-9} M, demonstrating three orders of magnitude enhancement in the LoD of Fabry–Pérot thin film biosensors. To the best of our knowledge this is the lowest LoD measured to date by any PSi biosensor for DNA.

3.1. Strengths and Limitations

The enhanced sensitivity of PSi-DNA biosensors is clearly evident under ITP focusing. Although we monitored DNA hybridization in a label-free format via RIFTS, the present assay employs fluorescently labeled DNA to allow visualization of the ITP peak location and its delivery to the reaction site. To avoid target labeling, any fluorophore with an electrophoretic mobility similar to that of the target (e.g., fluorescein for the case for DNA) can be added to the studied sample. Under the applied voltage, both the fluorophore and target molecules will isotachophoretically focus to allow the tracking of the unlabeled target peak position. Alternatively, the location of the ITP interface could be monitored by electric current readings.[64] The use of fluorescently labeled DNA also presented difficulties in determining the full dynamic range of the assay, as at low target concentrations ($<1 \times 10^{-9}$ M), the intensity of the ITP peak is too weak to be detected by our optical setup. Thus, the actual LoD of the ITP-$PSiO_2$ system may be lower than the values reported here. Further optimization in the dimensions of the $PSiO_2$ region, i.e., minimizing porous area to fit the microchannel (see Figure 1a), is expected to reduce target loss and improve the assay performance.

An important advantage of the current assay is the ability to analyze extremely small sample volumes (at 1×10^{-9} L range), which is critical for sample-limited applications. In spite of the small volume, ITP causes continuous accumulation of target molecules within a confined finite region, providing the biosensor with a high and nearly constant target supply.

This proof-of-concept study paves the way for further improvement in the sensitivity of PSi-based biosensors. While our demonstration here was limited to detection of DNA, the presented scheme is highly generic and has the potential to provide similar improvements in sensitivity for other charged target molecules.

4. Experimental Section

Materials: Highly doped p-type Si wafers (<100>-oriented, B-doped) were purchased from Sil'tronix Silicon Technologies (Archamps, France). Aqueous HF (48%) and ethanol absolute were supplied by Merck. The following chemicals: (3-aminopropyl)triethoxysilane (APTES), 4-(N-maleimidomethyl)cyclohexane-1-carboxylic acid 3-sulfo-N-hydroxysuccinimide ester sodium salt (Sulfo-SMCC), tris(2-carboxyethyl)phosphine hydrochloride (TCEP), *N*-(2-hydroxyethyl) piperazine-*N*′-(2-ethanesulfonic acid) (HEPES), bis(2-hydroxyethyl) amino-tris(hydroxymethyl) methane (BisTris), *N*-(tris(hydroxymethyl) methyl) glycine (Tricine), thiol-modified single-stranded DNA probe (ssDNA) (5′-TGATTCAAGCCGACT-Thiol-3′), fluorescein conjugated 100% complementary ssDNA (5′-AGTCGGCTTGAATCA-FITC-3′), and mismatch ssDNA (noncomplementary ssDNA) (5′-TGATTCAAGCCGACT-FITC-3′) were purchased from Sigma Aldrich (Rehovot, Israel). NaOH was obtained from Frutarom Ltd. (Haifa, Israel), NaCl from Bio-Lab Ltd. (Jerusalem, Israel), and magnesium chloride hexahydrate ($MgCl_2{\cdot}6H_2O$) was obtained from Avantor Performance Materials, Inc. (Center Valley, PA, USA). All solutions were prepared with Milli-Q water (18.2 MΩ cm). The SYLGARD 184 Silicon Elastomer kit, PDMS, was obtained from Dow Corning (Midland, USA).

Preparation and Characterization of Oxidized Porous Silicon Thin Films: Porous silicon thin films were prepared by electrochemical etching of a highly doped p-type crystalline Si wafer (0.0009 Ω cm) using a 3:1 (v/v) solution of aqueous HF (48%) and ethanol, respectively. A detailed description of the etching setup is reported elsewhere.[30] The anodization process was carried out in two steps. First a sacrificial layer was etched at a constant current density of 180 mA cm^{-2} for 30 s. The resulting porous layer was dissolved in a solution of aqueous NaOH (1 M) and ethanol at a ratio of 9:1 (v/v), respectively. Next, a subsequent etching at a constant current density of 385 mA cm^{-2} for 35 s was performed. After each step the silicon surface was thoroughly rinsed with ethanol and dried under a stream of nitrogen. The freshly etched porous silicon layer was then thermally oxidized in a tube furnace (thermolyne) at 1000 °C for 46 h under constant oxygen flow (0.5 L min^{-1}).

The structural properties, i.e., morphology and thickness, of the oxidized porous silicon ($PSiO_2$) layers were characterized by HRSEM using a Carl Zeiss Ultra Plus microscope, at an accelerating voltage of 1 keV. A secondary electrons detector was used to study the morphology and surface topography, while an energy selective backscattered (EsB) detector was employed to characterize the nanostructure composition. The spectroscopic liquid infiltration method (SLIM) was used in order to evaluate the porosity and layer thickness, as previously described.[32] Detailed description regarding the application of SLIM for the characterization of PSi-based nanomaterials can be found elsewhere.[10]

Fabrication and Assembly of the Microfluidic Device: The microchannels were fabricated using a soft lithography technique, according to standard protocols. An SU8 mold was fabricated at Stanford Microfluidic Foundry (Stanford University, Stanford, CA, http://www.stanford.edu/group/foundry/)[65] by standard lithography. Using the mold, microfluidic channels were fabricated in-house from PDMS at a polymer to cross-linker ratio of 10:1, followed by curing at 100 °C for 3 h. In order to achieve good adhesion between the PDMS and the SiO_2 substrate,

which includes both the planar oxide and the presilanized $PSiO_2$ region, the PDMS inner surface was exposed to oxygen plasma for 40 s (using a laboratory corona treater, BD-20V Electro-Technic Products), placed on top of the SiO_2 substrate, and then baked at 80 °C for 5 h.

Functionalization of Oxidized Porous Silicon: Prior to integration with the PDMS microchannels, the $PSiO_2$ was incubated with 4 vol% APTES in water/methanol (1:1 v/v) solution for 30 min. The surface was thoroughly rinsed with methanol and water and subsequently baked at 100 °C for 15 min. Subsequent surface modification steps were carried out after assembly, within the microchannels. All solutions were introduced into the microchannel using a vacuum pump and reactions were then performed under stationary conditions (no flow). Conjugation of the thiol-modified ssDNA probe (5′-TGATTCAAGCCGACT-Thiol-3′) to the amino-terminated $PSiO_2$ was performed according to previously reported protocols.[16,20] Briefly, the amino-terminated surface was incubated with a solution of sulfo-SMCC cross-linker (2 mg mL^{-1}) in HEPES buffer to form thiol active groups. The thiol-modified ssDNA (200×10^{-6} M) was reduced by TCEP in HEPES buffer prior to probe conjugation. After which, the activated DNA probe was introduced into the microchannel and incubated for 2 h. Subsequently, the DNA solution was removed and the channel was thoroughly rinsed with HEPES buffer and DI water.

Interferometric Reflectance Spectra Measurement and Fluorescence Imaging: To collect both the interferometric reflectance spectra and the fluorescent signal, we used a customized Zeiss upright microscope equipped with an Ocean Optics charge-coupled device (CCD) USB 4000 spectrometer. A two-port adapter was utilized to selectively transmit the light either to the collimator, which was coupled to a fiber-optic, or to the microscope camera (Axio Cam MRc, Zeiss). Figure S4 (Supporting Information) depicts an image of this experimental setup.

The $PSiO_2$-microfluidic device was fixed to the microscope stage under the objective. The light from a halogen source (halogen100 illuminator, Zeiss) was focused through an A-Plan objective (10×, 0.25 NA, Zeiss); the size of the illumination spot was controlled by the microscope iris and adjusted to the microchannel width, 350 μm in diameter, as shown in Figure S4 (Supporting Information). Both the illumination of the surface and the detection of the reflected light were performed perpendicular to the surface. Optical reflectivity spectra were collected using the CCD spectrometer and analyzed by applying FFT, as previously described by Massad-Ivanir et al.[32] In this work we present the optical data as relative ΔEOT, $\Delta EOT(t)/EOT_0 = (EOT(t) - EOT_0)/EOT_0$, where the term EOT_0 refers to the averaged EOT obtained during baseline establishment at the beginning of the optical experiments.

For real-time monitoring of ITP-based DNA hybridization, fluorescence imaging was carried out concurrently to the reflectivity measurements at a constant exposure time of 1.8 s using the camera. It should be emphasized that fluorescently labeled ssDNA was used for visualization of the ITP peak only, while the DNA detection was based on label-free Interferometric spectroscopy.

ITP-Based DNA Hybridization: In all ITP experiments the LE was composed of 100×10^{-3} M HCl, 200×10^{-3} M BisTris, 1×10^{-3} M MgCl. The TE was composed of 10×10^{-3} M Tricine and 20×10^{-3} M BisTris. The effect of the buffer composition on ITP efficiency has been extensively studied and optimized in previous works.[44,49,50] Briefly, the LE and TE buffers were chosen in order to maximize the sample focusing, while maintaining the buffer capacity and a pH value close to neutral, which is important for hybridization. In this work, we avoided suppression of electroosmotic flow (EOF) via passive or dynamic coatings, due to their possible effect on the optical readout (owing to their adsorption onto the $PSiO_2$ surface).

To perform the assay, we first filled the East reservoir (see Figure 1a) and the channel with LE buffer using a vacuum pump. We positioned the objective such that the reflectance spectra was collected from the $PSiO_2$ region of the channel, and flowed the buffer until a steady baseline was achieved. This readout location is then maintained throughout the experiment. We then rinsed the West reservoir with DI water several times and filled it with 27×10^{-6} L of TE buffer and 3×10^{-6} L of the target ssDNA. To initiate ITP, we applied a constant voltage of 350 V across the channel using a high-voltage sourcemeter (model 2410, Keithley Instruments) and recorded the current throughout the experiment. To control the location of the ITP focusing zone, we used pressure driven flow, produced by a water column connected to the East reservoir. The flow rate was controlled by modifying the water column height based on current reading, which is indicative of the zone's location along the channel.[66] The sample was allowed to focus at the ITP interface for ≈7 min before drawing the ITP plug to the $PSiO_2$ region by applying a negative pressure. Subsequently, in order to keep the ssDNA plug stationary on top of the $PSiO_2$ site, we applied positive pressure to counter electromigration. At this stage, the reflectance spectra was collected and analyzed in real-time in order to obtain the EOT values during the hybridization reaction. Once the EOT reached a constant value, the microchannel was rinsed with LE buffer using a vacuum pump to remove any unhybridized DNA molecules.

For comparison, we also monitored standard (no ITP) DNA hybridization in the $PSiO_2$-microfluidic device. In these experiments, a baseline EOT was obtained with LE buffer, followed by introduction of the complementary ssDNA (in LE Buffer) using a vacuum pump. Subsequently, the hybridization reaction was monitored under static conditions.

Supporting Information

Supporting Information is available from the Wiley Online Library or from the author.

Acknowledgements

This work was partially supported by the NEVET grant administered by the Russell Berrie Nanotechnology Institute (RBNI) and the Lorry I. Lokey Interdisciplinary Center for Life Sciences and Engineering (LS&E). M.B. gratefully acknowledges funding from the Israel Science Foundation (Grant No. 512/12 and 1698/12). E.S. gratefully acknowledges the support of the Israel Science Foundation (Grant 1146/12). The oxidation processes were performed at the Micro-Nano Fabrication Unit (MNFU), Technion. The authors thank Dr. Khaled Gommed for his assistance in preparation of the microfluidic channels.

Received: July 11, 2015
Revised: September 8, 2015
Published online: October 6, 2015

[1] K. P. S. Dancil, D. P. Greiner, M. J. Sailor, *J. Am. Chem. Soc.* **1999**, *121*, 7925.
[2] A. Janshoff, K.-P. S. Dancil, C. Steinem, D. P. Greiner, V. S.-Y. Lin, C. Gurtner, K. Motesharei, M. J. Sailor, M. R. Ghadiri, *J. Am. Chem. Soc.* **1998**, *120*, 12108.
[3] V. S. Lin, K. Motesharei, K. P. Dancil, M. J. Sailor, M. R. Ghadiri, *Science* **1997**, *278*, 840.
[4] A. Jane, R. Dronov, A. Hodges, N. H. Voelcker, *Trends Biotechnol.* **2009**, *27*, 230.
[5] K. A. Kilian, T. Böcking, J. J. Gooding, *Chem. Commun.* **2009**, *6*, 630.
[6] S. M. Weiss, G. Rong, J. L. Lawrie, *Physica E* **2009**, *41*, 1071.
[7] L. De Stefano, L. Rotiroti, I. Rea, L. Moretti, G. Di Francia, E. Massera, A. Lamberti, P. Arcari, C. Sanges, I. Rendina, *J. Optics A: Pure Appl. Optics* **2006**, *8*, S540.
[8] L. A. DeLouise, P. M. Kou, B. L. Miller, *Anal. Chem.* **2005**, *77*, 3222.
[9] C. Jamois, C. Li, E. Gerelli, Y. Chevolot, V. Monnier, R. Skryshevskyi, R. Orobtchouk, E. Souteyrand, T. Benyattou, in *Proc. SPIE 7713, Photonic Crystal Materials and Devices IX*, SPIE, Bellingham, WA, USA, **2010**, 77130U.

[10] M. J. Sailor, *Porous Silicon in Practice: Preparation, Characterization and Applications*, Wiley-VCH, Weinheim, Germany **2012**.
[11] V. Torres-Costa, R. J. Martin-Palma, in *Porous Silicon for Biomedical Applications*, (Ed: H. A. Santos), Woodhead Publishing Ltd., Sawston, Cambridge **2014**, Ch. 8.
[12] G. Shtenberg, E. Segal, in *Handbook of Porous Silicon* (Ed: L. Canham), Springer International Publishing, Switzerland **2014**, Ch. 87.
[13] L. De Stefano, P. Arcari, A. Lamberti, C. Sanges, L. Rotiroti, I. Rea, I. Rendina, *Sensors* **2007**, *7*, 214.
[14] L. Moretti, I. Rea, L. De Stefano, I. Rendina, *Appl. Phys. Lett.* **2007**, *90*, 191112.
[15] C. Pacholski, M. Sartor, M. J. Sailor, F. Cunin, G. M. Miskelly, *J. Am. Chem. Soc.* **2005**, *127*, 11636.
[16] G. Rong, J. D. Ryckman, R. L. Mernaugh, S. M. Weiss, *Appl. Phys. Lett.* **2008**, *93*, 161109.
[17] J. D. Ryckman, M. Liscidini, J. E. Sipe, S. M. Weiss, *Appl. Phys. Lett.* **2010**, *96*, 171103.
[18] G. Rong, A. Najmaie, J. E. Sipe, S. M. Weiss, *Biosens. Bioelectron.* **2008**, *23*, 1572.
[19] M. A. Anderson, A. Tinsley-Bown, P. Allcock, E. A. Perkins, P. Snow, M. Hollings, R. G. Smith, C. Reeves, D. J. Squirrell, S. Nicklin, *Phys. Status Solidi* **2003**, *197*, 528.
[20] G. Rong, S. M. Weiss, *Phys. Status Solidi* **2009**, *206*, 1365.
[21] M. R. Lee, P. M. Fauchet, *Opt. Express* **2007**, *15*, 4530.
[22] M. M. Orosco, C. Pacholski, G. M. Miskelly, M. J. Sailor, *Adv. Mater.* **2006**, *18*, 1393.
[23] G. A. Rodriguez, J. D. Ryckman, Y. Jiao, S. M. Weiss, *Biosens. Bioelectron.* **2014**, *53*, 486.
[24] X. Wei, S. M. Weiss, *Opt. Express* **2011**, *19*, 11330.
[25] C. Steinem, A. Janshoff, V. S. Y. Lin, N. H. Völcker, M. R. Ghadiri, *Tetrahedron* **2004**, *60*, 11259.
[26] H. Zhang, Z. Jia, X. Lv, J. Zhou, L. Chen, R. Liu, J. Ma, *Biosens. Bioelectron.* **2013**, *44*, 89.
[27] Y. Zhao, J. L. Lawrie, K. R. Beavers, P. E. Laibinis, S. M. Weiss, *ACS Appl. Mater. Interfaces* **2014**, *6*, 13510.
[28] M. Y. Chen, M. D. Klunk, V. M. Diep, M. J. Sailor, *Adv. Mater.* **2011**, *23*, 4537.
[29] H. Ouyang, L. A. DeLouise, B. L. Miller, P. M. Fauchet, *Anal. Chem.* **2007**, *79*, 1502.
[30] K. Urmann, J. G. Walter, T. Scheper, E. Segal, *Anal. Chem.* **2015**, *87*, 1999.
[31] G. Shtenberg, N. Massad-Ivanir, O. Moscovitz, S. Engin, M. Sharon, L. Fruk, E. Segal, *Anal. Chem.* **2013**, *85*, 1951.
[32] N. Massad-Ivanir, G. Shtenberg, T. Zeidman, E. Segal, *Adv. Funct. Mater.* **2010**, *20*, 2269.
[33] H. Pei, X. Zuo, D. Pan, J. Shi, Q. Huang, C. Fan, *NPG Asia Mater.* **2013**, *5*, e51.
[34] J. Wang, *Nucl. Acids Res.* **2000**, *28*, 3011.
[35] G. A. Rodriguez, J. L. Lawrie, S. M. Weiss, in *Porous Silicon for Biomedical Applications*, (Ed: H. A. Santos), Woodhead Publishing Ltd., Sawston, Cambridge, UK **2014**, Ch. 13.
[36] L. De Stefano, G. Oliviero, J. Amato, N. Borbone, G. Piccialli, L. Mayol, I. Rendina, M. Terracciano, I. Rea, *J. R. Soc. Interface* **2013**, *10*, 20130160.
[37] I. Rea, E. Orabona, A. Lamberti, I. Rendina, L. De Stefano, *Biomicrofluidics* **2011**, *5*, 034120.
[38] X. Wei, J. W. Mares, Y. Gao, D. Li, S. M. Weiss, *Biomed. Opt. Exp.* **2012**, *3*, 1993.
[39] Y. Zhao, J. L. Lawrie, P. E. Laibinis, S. M. Weiss, in *Proc. SPIE BiOS 8933, Frontiers in Biological Detection: From Nanosensors to Systems VI*, SPIE, Bellingham, WA, USA, **2014**, 893302.
[40] L. De Stefano, E. Orabona, A. Lamberti, I. Rea, I. Rendina, *Sens. Actuators, B* **2013**, *179*, 157.
[41] L. De Stefano, I. Rea, in *Handbook of Porous Silicon*, (Ed: L. Canham), Springer International Publishing, Switzerland **2014**, Ch. 81.
[42] V. M. Ugaz, J. L. Christensen, in *Microfluidic Technologies for Miniaturized Analysis Systems*, (Eds: S. Hardt, F. Schonfeld), Springer US, New York, USA **2007**, Ch. 10.
[43] G. M. Whitesides, *Nature* **2006**, *442*, 368.
[44] M. Bercovici, C. M. Han, J. C. Liao, J. G. Santiago, *Proc. Natl. Acad. Sci. USA* **2012**, *109*, 11127.
[45] G. Garcia-Schwarz, A. Rogacs, S. S. Bahga, J. G. Santiago, *J. Visual. Exp.* **2012**, DOI: 10.3791/3890.
[46] B. Jung, R. Bharadwaj, J. G. Santiago, *Anal. Chem.* **2006**, *78*, 2319.
[47] M. Bercovici, G. V. Kaigala, K. E. Mach, C. M. Han, J. C. Liao, J. G. Santiago, *Anal. Chem.* **2011**, *83*, 4110.
[48] Y. Cong, D. Bottenus, B. Liu, S. B. Clark, C. F. Ivory, *Electrophoresis* **2014**, *35*, 646.
[49] M. Karsenty, S. Rubin, M. Bercovici, *Anal. Chem.* **2014**, *86*, 3028.
[50] T. Rosenfeld, M. Bercovici, *Lab Chip* **2014**, *14*, 4465.
[51] C.-Y. Wu, O. Adeyiga, J. Lin, D. Di Carlo, *Lab Chip* **2014**, *14*, 3258.
[52] T. Jalkanen, E. Mäkilä, Y. I. Suzuki, T. Urata, K. Fukami, T. Sakka, J. Salonen, Y. Ogata, *Adv. Funct. Mater.* **2012**, *22*, 3890.
[53] M. P. Stewart, J. M. Buriak, *Adv. Mater.* **2000**, *12*, 859.
[54] K. Wang, G. Liu, N. Hoivik, E. Johannessen, H. Jakobsen, *Chem. Soc. Rev.* **2014**, *43*, 1476.
[55] A. E. Pap, K. Kordás, G. Tóth, J. Levoska, A. Uusimäki, J. Vähäkangas, S. Leppävuori, T. F. George, *Appl. Phys. Lett.* **2005**, *86*, 041501.
[56] G. Gaur, D. S. Koktysh, S. M. Weiss, *Adv. Funct. Mater.* **2013**, *23*, 3604.
[57] J. Riikonen, M. Salomäki, J. van Wonderen, M. Kemell, W. Xu, O. Korhonen, M. Ritala, F. MacMillan, J. Salonen, V.-P. Lehto, *Langmuir* **2012**, *28*, 10573.
[58] G. Shtenberg, N. Massad-Ivanir, L. Fruk, E. Segal, *ACS Appl. Mater. Interfaces* **2014**, *6*, 16049.
[59] C. K. Tsang, T. L. Kelly, M. J. Sailor, Y. Y. Li, *ACS Nano* **2012**, *6*, 10546.
[60] V. Labunov, V. Bondarenko, I. Glinenko, A. Dorofeev, L. Tabulina, *Thin Solid Films* **1986**, *137*, 123.
[61] G. Müller, M. Nerding, N. Ott, H. Strunk, R. Brendel, *Phys. Status Solidi* **2003**, *197*, 83.
[62] N. Ott, M. Nerding, G. Müller, R. Brendel, H. Strunk, *Phys. Status Solidi* **2003**, *197*, 93.
[63] T. H. Nguyen, M. Elimelech, *Biomacromolecules* **2007**, *8*, 24.
[64] M. Karsenty, T. Rosenfeld, K. Gommed, M. Bercovici, *Anal. Chem.* **2015**, *87*, 388.
[65] D. Gerber, S. J. Maerkl, S. R. Quake, *Nat. Methods* **2009**, *6*, 71.
[66] N. Reinhoud, U. Tjaden, J. Van der Greef, *J. Chromatogr. A* **1994**, *673*, 239.